Journal of Asian Earth Sciences 90 (2014) 101–106

Contents lists available at ScienceDirect

Journal of Asian Earth Sciences

journal homepage: www.elsevier.com/locate/jseaes

Seismic behavior in central Taiwan: Response to stress evolution following the 1999 M_w 7.6 Chi-Chi earthquake

Chung-Han Chan [a,b,*], Yih-Min Wu [a]

[a] Department of Geosciences, National Taiwan University, Taipei, Taiwan
[b] Earth Observatory of Singapore, Nanyang Technological University, Singapore

ARTICLE INFO

Article history:
Received 2 December 2013
Received in revised form 25 March 2014
Accepted 8 April 2014
Available online 2 May 2014

Keywords:
Chi-Chi earthquake
Coulomb stress change
Afterslip
Viscoelastic relaxation
Taiwan

ABSTRACT

Following the 1999 M_w 7.6 Chi-Chi earthquake, a large amount of seismicity occurred in the Nantou region of central Taiwan. Among the seismic activities, eight $M_w \geqslant 5.8$ earthquakes took place following the Chi-Chi earthquake, whereas only four earthquakes with comparable magnitudes took place from 1900 to 1998. Since the seismicity rate during the Chi-Chi postseismic period has never returned to the background level, such seismicity activation cannot simply be attributed to modified Omori's Law decay. In this work, we attempted to associate seismic activities with stress evolution. Based on our work, it appears that the spatial distribution of the consequent seismicity can be associated with increasing coseismic stress. On the contrary, the stress changes imparted by the afterslip; lower crust–upper mantle viscoelastic relaxation; and sequent events resulted in a stress drop in most of the study region. Understanding seismogenic mechanisms in terms of stress evolution would be beneficial to seismic hazard mitigation.

1. Introduction

Two large earthquakes struck the Nantou region of central Taiwan in 2013. A M_w 5.8 earthquake occurred on March 27th, 2013 (Fig. 1). The Central Weather Bureau Seismic Network (CWBSN) observed the largest intensity of VI near the epicenter. The event resulted in one fatality, ninety-seven injuries, and loss of property. Two months later, on June 2nd, another earthquake of M_w 6.3 took place in the vicinity (Fig. 1). The event caused a comparable intensity and led to a loss of property and human life. In addition to these two events in 2013, another six earthquakes with $M_w \geqslant 6.0$ took place in this region following the 1999 M_w 7.6 Chi-Chi earthquake (Fig. 1). For the purpose of seismic hazard mitigation, it is crucial to determine seismogenic mechanisms in this region.

Seismic behaviors could be controlled by stress evolution. Ma et al. (2005) calculated the Coulomb stress change (ΔCFS) imparted by the Chi-Chi coseismic ruptures, and analyzed seismicity in Taiwan during the subsequent 53 months. They concluded that during this period the ΔCFS caused by the Chi-Chi earthquake dominated Taiwan seismic activities. Chan and Stein (2009) evaluated the stress evolution imparted by the afterslip, the viscoelastic relaxation, and consequent earthquakes during the postseismic period and determined that post-seismic stress changes play an important role on the influence of seismic behaviors in Taiwan. Such studies are critical for understanding the correlations between stress evolution with seismic activities during the first years of the postseismic period. The time period from the Chi-Chi earthquake to the 2013 Nantou earthquake sequence is approximately 13 years. The stress influenced by the Chi-Chi earthquake could still be controlling the 2013 Nantou earthquake sequence, and understanding the earthquake source mechanism is critical. Therefore, in this study, we sought to associate seismic activity with stress evolution in central Taiwan. We first investigated the spatial–temporal distribution of seismicity. Then, the ΔCFS during the Chi-Chi coseismic and postseismic periods was evaluated. Through statistical comparisons, the mechanisms driving seismicity within the region are expected to become clearer.

2. Seismic activity

2.1. The CWBSN catalog

The Central Weather Bureau Seismic Network (CWBSN) has started monitoring seismic activity within Taiwan in the beginning of the 1990s (Wu et al., 2008). Due to the change in recording mode from a triggered recording to a continuous one, the CWBSN has

* Corresponding author at: Earth Observatory of Singapore, Nanyang Technological University, Singapore. Tel.: +65 65921771.
E-mail address: hantijun@googlemail.com (C.-H. Chan).

http://dx.doi.org/10.1016/j.jseaes.2014.04.006
1367-9120/

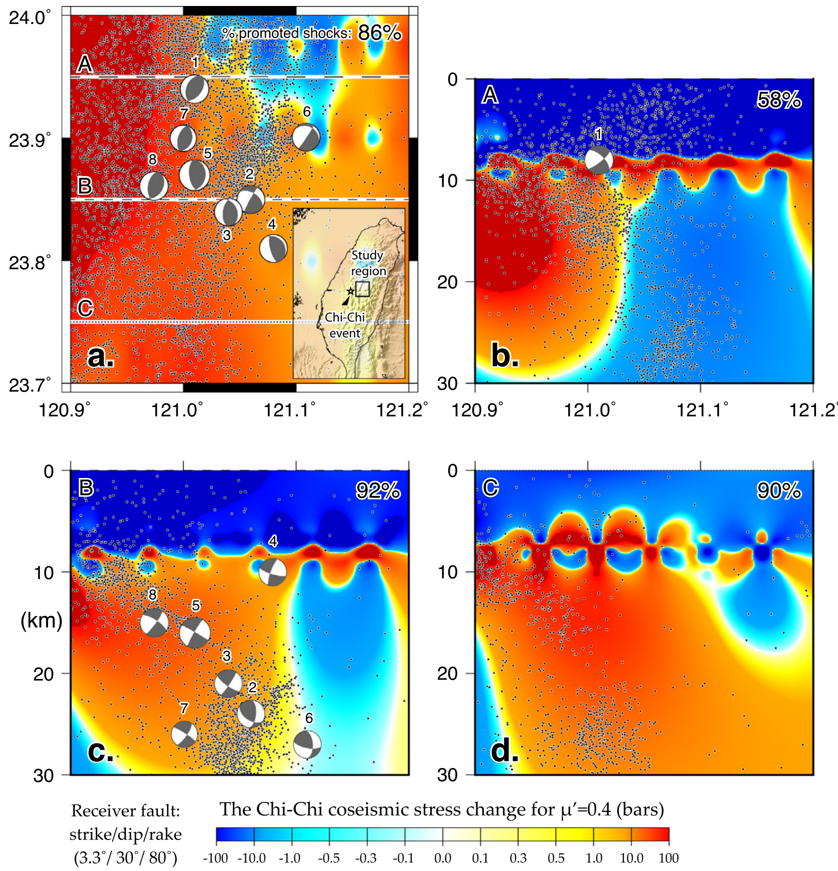

Fig. 1. The maximum ΔCFS (a) at the depth of 10–20 km, (b) at the Latitude of 23.9–24.0°, (c) at the Latitude of 23.8–23.9°, and (d) at the Latitude of 23.7–23.8° during the Chi-Chi coseismic period. The corresponding seismicity that occurred following the Chi-Chi earthquake is superimposed. The ratios of seismicity in the stress-increase regions are shown. The series number of each earthquake is presented in Table 2.

greatly enhanced earthquake-monitoring ability since 1993 (Wu and Chiao, 2006). In order to comprehend the reliability of the catalog within the study region, the temporal distribution of the magnitude of completeness (M_c) was evaluated based on the maximum curvature approach (Wiemer and Wyss, 2000). Earthquakes with focal depths $\leqslant$ 30 km during the period from 1993 to 2012 were considered. The M_c was kept as low as $\leqslant$2.0 for most of the periods (Fig. 2b). The only exception took place following the Chi-Chi earthquake. A reduction in seismic detection ability can be attributed to seismicity bursts following a large earthquake. For the use of the catalog, a magnitude threshold of 2.0 was considered.

2.2. The spatial and temporal distribution of seismicity

The spatial distribution of seismicity in Nantou was determined. A higher rate was observed in the northwestern portion of the study region (Fig. 1a). The profiles (Fig. 1b–d) represent the distribution of seismicity with depth. An eastern dipping trend of seismicity corresponds to the focal mechanisms of large events. Most events take place at the depth between 8 and 30 km. The depth distribution of seismicity is summarized in Table 1. The focal depths of $M \geqslant 2.0$ earthquakes are generally between 5 and 30 km. Additionally, for events with a larger magnitude, lower seismicity ratios were observed at a depth less than 10 km.

In Fig. 2a, the temporal evolution of the seismicity rate within the study region is presented in the form of a time series. A sudden rise in the seismicity rate following the Chi-Chi earthquake could be associated with a consequent aftershock sequence (Chang et al., 2000; Chang et al., 2007). Since the seismicity rate during the Chi-Chi postseismic period has never returned to the background level (solid line prior to the Chi-Chi earthquake in Fig. 2a), such a temporal trend cannot simply be explained by modified Omori's Law (Utsu, 1961), suggesting that the seismicity rate returns to background after a certain period.

3. The association of consequent earthquakes with the Chi-Chi coseismic stress change

Previous studies (e.g., Chan and Wu, 2012; Chan et al., 2012) have suggested that a positive Coulomb stress change (ΔCFS) encourages the occurrence of consequent events and a negative ΔCFS inhibits future seismicity. In the following, the relationship between the Chi-Chi coseismic stress change and the distribution of consequent earthquakes will be discussed. For this purpose, the procedure of the ΔCFS calculation is introduced. The Chi-Chi coseismic ΔCFS on the focal mechanisms of large earthquakes and within the Nantou region are then evaluated.

3.1. The Coulomb stress change (ΔCFS) imparted by the Chi-Chi coseismic slip

According to previous studies (Harris (1998) and references therein), the ΔCFS can be represented, as follows:

$$\Delta CFS = \Delta\tau + \mu'\Delta\sigma_n, \quad (1)$$

where $\Delta\tau$ is the change of the shear stress along the rupture direction on the receiver fault; μ' is the apparent friction coefficient; and

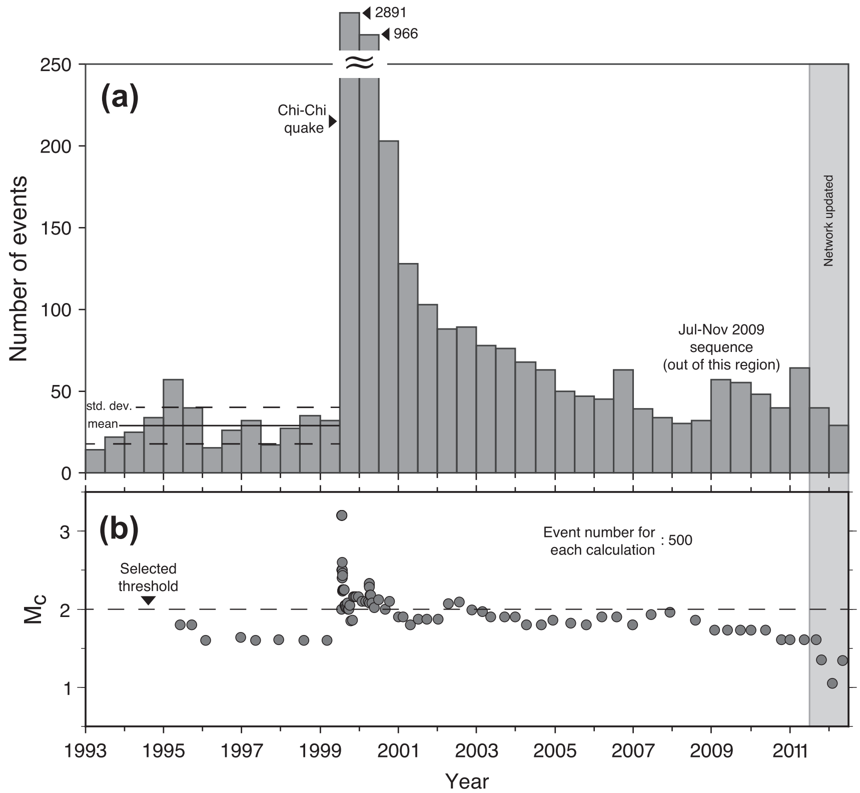

Fig. 2. (a) The number of $M \geqslant 2.0$ seismicity and (b) the magnitude of completeness, (M_c), as a function of time within the study region. Note that due to the update of the seismic network since 2012, the determined magnitudes are lower than the previously determined magnitudes.

Table 1
The depth distributions for seismicity with different magnitude thresholds and volumes of ΔCFS ⩾ 0.1 bars.

Depth range (km)	After Chi-Chi seismicity			ΔCFS ⩾ 0.1 bar (%)
	$M \geqslant 2.0$ (%)	$M \geqslant 4.0$ (%)	$M \geqslant 5.0$ (%)	
0–5	6	3	0	1
5–10	17	15	7	37
10–15	26	41	48	65
15–20	12	16	29	59
20–25	16	13	10	59
25–30	23	12	7	48

$\Delta\sigma_n$ is the change of the normal stress perpendicular to the receiver fault (unclamping is positive). In order to estimate ΔCFS, the COULOMB 3.3 program (Toda and Stein, 2002) is applied.

For the calculation of ΔCFS during the Chi-Chi coseismic period, a coseismic slip model was required. Here, the Chi-Chi coseismic slip model by Johnson and Segall (2004) was considered. The model obtains a four-plane fault geometry with a sub-horizontal décollment at the depth of 7.7 km, and also explains GPS deformation.

3.2. The stress resolved on the focal mechanisms of large earthquakes

Based on various references, the source parameters of eight significant earthquakes were obtained (Table 2). Although there are two conjugation planes for a focal mechanism, based on the dipping trend of seismicity (Fig. 1b and c), the eastern dipping plane of each earthquake was assumed as the actual one of interest. The ΔCFS on each focal plane was evaluated (Table 2). Seven of the eight (88%) events could be associated with the Chi-Chi coseismic stress increase, suggesting that the Chi-Chi promoted the rupture of seismotectonics within the Nantou region.

3.3. A comparison with the distribution of smaller events

The spatial distribution of the Chi-Chi coseismic ΔCFS was evaluated and indicated that the stress above the décollement (depth ⩽ 7.7 km) was dropped; in contrast, the stress in most of the areas beneath the décollement was promoted (Fig. 1b–d). Such a result corresponds to the characteristic ΔCFS pattern for a ramp-décollment structure (Fig. 4 of Chan and Stein (2009)). To quantify the ΔCFS distribution with depth, we calculated ΔCFS in each 1 km * 1 km * 1 km cell. The proportions of the region with an increased ΔCFS at different depth bins are represented in Table 1, showing a ΔCFS increase in more than 50% of the regions at the depth between 10 and 25 km. By contrast, at a depth of 0–5 and 5–10 km the ratios of regions that are stress-promoted were significantly low (1% and 37%, respectively).

The Chi-Chi coseismic ΔCFS may well explain the spatial distribution of the seismicity (Fig. 1). Few of the events were in the region with a ΔCFS drop. For the $M \geqslant 2.0$ events, only 23% were at a depth ⩽ 10 km, whereas most of the regions were further from the next failure (Table 1). Note that these ratios were even lower for events with larger magnitudes (i.e., 18% and 7% for $M \geqslant 4.0$ and 5.0, respectively).

Table 2
The earthquake parameters of the Nantou sequence and the corresponding ΔCFS imparted by the Chi-Chi coseismic slip and preceding earthquake(s). The reference of each earthquake parameter is presented.

No.	Date (year/month/date)	Longitude (°)	Latitude (°)	Depth (km)	M_w	Strike (°)	Dip (°)	Rake (°)	Reference	Chi-Chi ΔCFS, bars	Nantou seq. ΔCFS, bars
1	99/09/20	121.01	23.94	8	6.4	36	50	100	Chi and Dreger (2004)	0.3	–
2	99/09/20	121.06	23.85	24	6.1	209	85	139	Yen (2002)	0.05	−0.07
3	99/09/20	121.04	23.84	21	6.1	336	38	63	Yen (2002)	1.29	−12.62
4	99/09/22	121.08	23.81	10	6.2	318	22	64	Chi and Dreger (2004)	2.83	1.13
5	99/09/25	121.01	23.87	16	6.8	5	30	100	Chi and Dreger (2004)	3.14	−6.82
6	00/06/10	121.11	23.9	27	6.1	33	87	−114	BATS	−2.23	1.61
7	13/03/27	121.00	23.9	26	5.8	14	34	87	BATS	0.77	1.92
8	13/06/02	120.97	23.86	15	6.3	30	37	106	BATS	3.88	−3.32

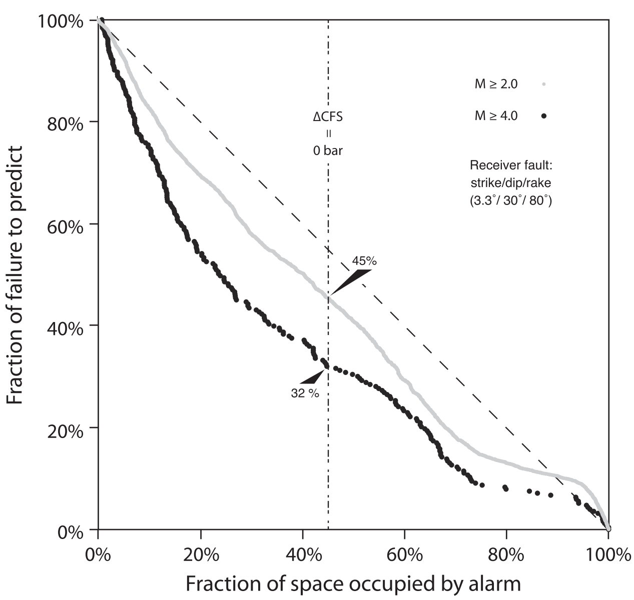

Fig. 3. A Molchan diagram – which investigates the correlation between the Chi-Chi coseismic ΔCFS and the consequent seismicity during September 1999 and May 2013. The various colors represent the seismicity with different magnitude thresholds.

The relationship between the ΔCFS and the consequent earthquake was also statistically tested using the Molchan diagram (Molchan, 1990). In this diagram, the "fraction of space occupied by alarm" indicated ratios of the study region with a ΔCFS level equal to or higher than a threshold (defined as "alarm"). The "fraction of failure to predict" presents the ratios of consequent earthquakes having a lower ΔCFS level than the alarm. In other words, when the data points are distributed along the diagonal line, the distribution of target earthquakes are independent of the ΔCFS. A convex distribution suggests that the majority of the consequent earthquakes occurred within regions with a lower ΔCFS as compared to the entire area. Whereas, a concavity suggests that most of the consequent earthquakes were higher in the ΔCFS area. The Molchan diagram confirmed the relationship between the distributions of consequent seismicity and the ΔCFS (Fig. 3). Additionally, a better correlation was obtained for larger earthquakes. Only 45% and 32% of seismicity with a magnitude $M \geqslant 2.0$ and 4.0, respectively, were found within the ΔCFS drop area that covers 55% of the entire study region.

4. Stress evolution during the Chi-Chi postseismic period

In the discussion above, we proved that Chi-Chi coseismic ΔCFS controls seismic activity within the study region. Next, we try to associate the seismicity with stress evolution during the postseismic period. We evaluate and discuss the stress imparted by some of the postseismic factors (i.e., afterslip, lower crust–upper mantle viscoelastic rebound, and earthquakes of the Nantou sequence).

To evaluate the ΔCFS by the afterslip, the model inferred by Yu et al. (2003) was introduced. The model fulfilled GPS observations during the first 15 months of the Chi-Chi postseismic period. The afterslip results in a ΔCFS drop in most parts of the Nantou region (Fig. 4a). Additionally, seven of the eight significant events were located within the stress drop region, suggesting that the seismic behaviors are not controlled by the afterslip. In addition, the

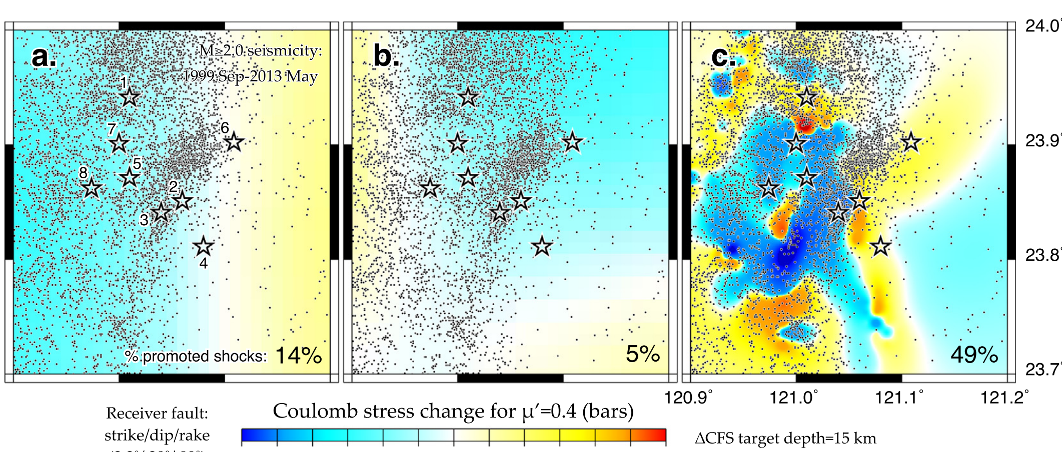

Fig. 4. The ΔCFS imparted by (a) the afterslip, (b) the viscoelastic relaxation, and (c) preceding events during the Chi-Chi postseismic period. The target depth for the ΔCFS calculation was 15 km. We confirmed that the ΔCFSs due to afterslip and viscoelastic relaxation were insensitive to depth. The series number of each earthquake and the corresponding ΔCFS imparted by the preceding earthquake(s) are presented in Table 2.

occurrence of smaller events cannot be associated with afterslip triggering. Only 14% of the $M \geqslant 2.0$ events are within the region where stress is increased by afterslip.

For the calculation of stress evolution by viscoelastic relaxation, the rheology model inferred by Chan and Stein (2009) was implemented (Fig. 3c of the reference). We evaluated the stress change 14 years after the 1999 Chi-Chi earthquake and found that stress status is further away from failure in almost the entire study region (Fig. 4b). Furthermore, all of the significant events as well as 95% of the $M \geqslant 2.0$ ones were located within the stress drop region. The results suggest that seismic activity does not fulfill the viscoelastic rebound model.

In addition to the Chi-Chi earthquake, the events of the Nantou sequence may also alter the stress status and dominate the behaviors of consequent earthquakes. Since the ΔCFSs imparted by small earthquakes are trivial (Ma et al., 2005), we only evaluated ΔCFS using the eight significant events (Fig. 4c). Calculation of the ΔCFS requires knowledge of the rupture parameters for source events (i.e., the geometry of the rupturing fault and the magnitude of the slip). The detailed slip dislocation models for the Nos. 1, 4, and 5 events were obtained by Chi and Dreger (2004). For the remaining events, we adopted a homogenous slip model using the dimensions and average slips according to the scaling laws of Yen and Ma (2011). Stress in half of the region is promoted, making it difficult to distinguish their correlation with seismicity patterns. 49% of the $M \geqslant 2.0$ postseismic events are located in the region where stress is enhanced by previous events. To further determine the interactions between significant events, the ΔCFS for each focal plane using preceding events was calculated (Table 2). Only three of the seven events (43%) were found to be promoted.

5. Discussion and conclusion

5.1. Seismicity remains higher than background following the Chi-Chi earthquake

Previous studies (e.g., Chang et al. (2000) and references therein) have observed a large amount of aftershocks in the vicinity of the 1999 Chi-Chi rupture zone. Seismicity rates within parts of central Taiwan have returned at a background level several years following the Chi-Chi earthquake (Ma et al., 2005). In this study, in contrast, we observed that the seismicity rate within the Nantou region remained higher than background (Fig. 2). Additionally, in comparison to eight significant events since 1999 (annual rate: 0.57), only four earthquakes with $M \geqslant 6.0$ took place from 1900 to 1998 (annual rate: 0.04).

5.2. The role of coseismic stress change in controlling seismicity during postseismic period

The seismicity rate increase could be attributed to the Chi-Chi coseismic stress increase. The coseismic ΔCFS also explained the detailed distribution of seismicity along the depth (Fig. 1b–d). An increase in ΔCFS was calculated beneath the décollement (at a depth $\geqslant$ 10 km); whereas, the stress above was determined to be dropped. In comparison, 77% of $M \geqslant 2.0$ events were located at a depth $\leqslant$ 10 km, whereas most were closer to the next failure (Table 1). That the fault(s) beneath the décollement (Yue et al., 2005) or the lower part of the Shuilikeng Fault (Camanni et al., 2013) have been activated following the Chi-Chi earthquake has been suggested. Additionally, these ratios are even higher for larger events (82% and 93% for $M \geqslant 4.0$ and 5.0, respectively). Using the Molchan diagram (Fig. 3), the correlations between coseismic ΔCFS and consequent seismicity were confirmed. Additionally, seismicity with larger magnitudes had a better correlation (black dots in Fig. 3). The phenomenon may be attributed to a more precise depth location for large events and/or more heterogeneous rupture mechanisms for small events.

5.3. The role of postseismic stress evolution in controlling seismicity during postseismic period

Contrary to the coseismic ΔCFS, the correlation between stress evolutions during the postseismic period with consequent seismicity was trivial. The stress changes imparted by afterslip; lower crust–upper mantle viscoelastic rebound; and the events of the Nantou sequence were evaluated (Fig. 4). All of these factors were determined to result in a stress decrease in most of the Nantou region. Additionally, most of the events from 1999 and 2013 were found within the postseismic stress drop zone. The interactions between the significant events of the Nantou sequence were examined (Table 2). The results concluded that few (43%) of them were promoted by preceding events. Here, it should be noted that inaccuracy in the ΔCFS calculation may be attributed to the homogeneous slip dislocation models for Nos. 2, 3, 6, 7, and 8 events. The correlations between postseismic stress evolution and consequent seismicity were evaluated statistically through the Molchan diagram (Fig. 5). The stress change imparted by each of the postseismic factors represented negative correlation with distribution of the earthquakes (most of dots in the diagram are above the diagonal line).

It is been aware that time-dependent stress evolutions were not presented and discussed in detail in this study. The 15-month afterslip model of Yu et al. (2003) was implemented. According to the GPS observations, however, the afterslip posterior to this period is trivial (Yu et al., 2003). Regarding visco-elastic rebound, although the magnitudes of stress change for various periods are different, but their patterns are similar (Fig. 6). For all of the time periods, most of the events were located within the stress drop region.

5.4. The possible application of time-dependent probabilistic seismic hazard assessments

We concluded that the Chi-Chi coseismic ΔCFS dominated seismic activity within the Nantou region. If the rate-and-state friction

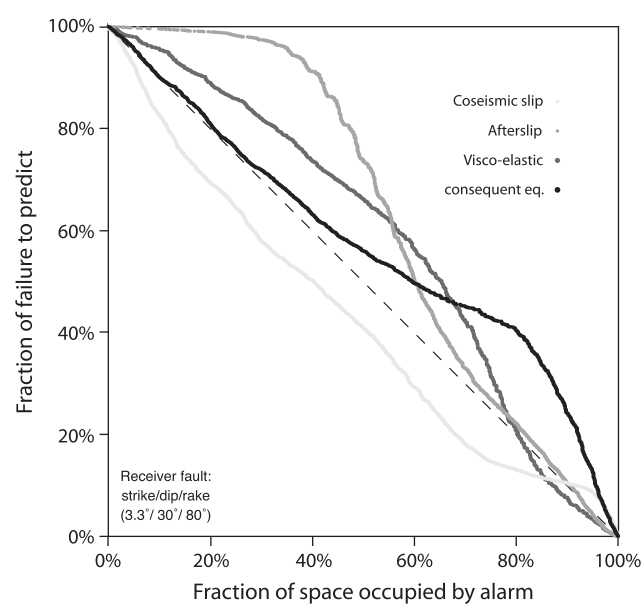

Fig. 5. A Molchan diagram – which investigates the correlation between the ΔCFS by different factors and the consequent seismicity. The various colors represent the ΔCFS by varies factors.

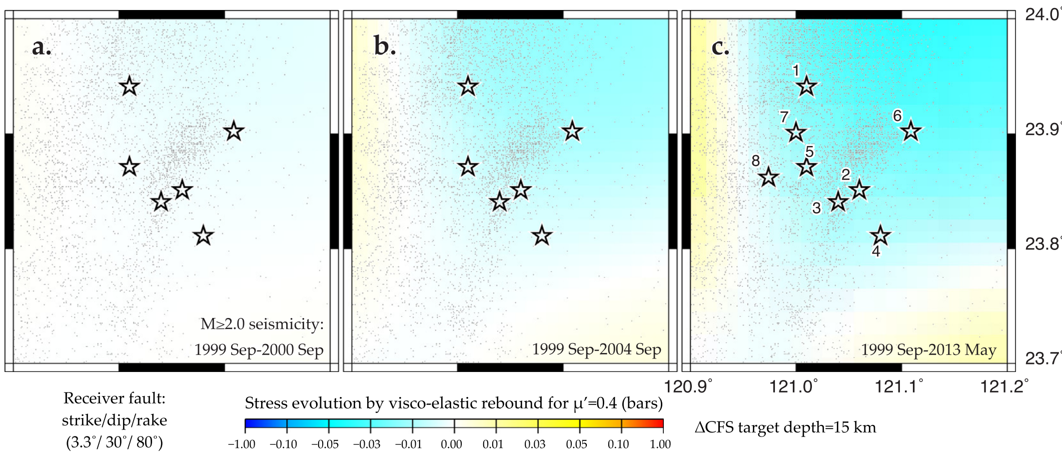

Fig. 6. The ΔCFS imparted by the viscoelastic relaxation for (a) 1 year, (b) 5 years, and (c) 13 years in the postseismic period. The seismicity during the corresponding periods is superimposed. The series number of each earthquake and the corresponding ΔCFS imparted by the preceding earthquake(s) are presented in Table 2.

model (Dieterich, 1994) is further implemented, spatial and temporal distributions of the seismicity rate can be quantified (e.g., Toda and Enescu, 2011; Chan et al., 2012). The application of the rate-and-state friction model requires determination of corresponding parameters (e.g., a constitutive parameter of the model, aftershock duration, and tectonic shear stressing rate). It is beyond the scope of this study. Additionally, by considering ground motion attenuation behaviors from ground motion prediction equations or waveform simulations, time-dependent seismic hazards can be assessed (Chan et al., 2013). Such information provides important information for decision-makers and public officials in respect to seismic hazard mitigation (McGuire, 2001).

Acknowledgement

Our work was supported by the National Science Council in Taiwan.

References

Camanni, G., Brown, D., Alvarez-Marron, J., Wu, Y.M., Chen, H.A., 2013. The Shuilikeng fault in the central Taiwan mountain belt. J. Geological Soc., London 171, 117–130. doi: 10.1144/jgs2013-014.

Chan, C.H., Stein, R.S., 2009. Stress evolution following the 1999 Chi-Chi, Taiwan, earthquake: consequences for afterslip, relaxation, aftershocks, and departures from Omori decay. Geophys. J. Int. doi: 10.1111/j.1365-246X.2008.04069.x.

Chan, C.H., Wu, Y.M., 2012. The burst of seismicity after the 2010 M6.4 Jiashian earthquake and its implication of short-term seismic hazard in southern Taiwan. J. Asian Earth Sci. 51, 231–239. http://dx.doi.org/10.1016/j.jseaes.2012.08.011.

Chan, C.H., Wu, Y.M., Wang, J.-P., 2012. Earthquake forecasting through a smoothing Kernel and the rate-and-state friction law: application to the Taiwan region. Nat. Hazards Earth Syst. Sci. 12, 1–13. http://dx.doi.org/10.5194/nhess-12-1-2012.

Chan, C.H., Wu, Y.M., Cheng, C.T., Lin, P.S., Wu, Y.C., 2013. Time-dependent probabilistic seismic hazard assessment and its application to Hualien City, Taiwan. Nat. Hazards Earth Syst. Sci. 13, 1–16. http://dx.doi.org/10.5194/nhess-13-1-2013.

Chang, C.-H., Wu, Y.-M., Shin, T.-C., Wang, C.-Y., 2000. Relocation of the 1999 Chi-Chi Earthquake in Taiwan. Terr., Atmospheric Oceanic Sci. 11 (3), 581–590.

Chang, C.-H., Wu, Y.-M., Zhao, L., Wu, F.T., 2007. Aftershocks of the 1999 Chi-Chi, Taiwan, earthquake: the first hour. Bull. Seismol. Soc. Am. 97, 1245–1258. http://dx.doi.org/10.1785/0120060184.

Chi, W.-C., Dreger, D., 2004. Crustal deformation in Taiwan: results from finite source inversions of six $M_W > 5.8$ Chi-Chi aftershocks. J. Geophys. Res. 109, B07305. http://dx.doi.org/10.1029/2003JB002606.

Dieterich, J.H., 1994. A constitutive law for rate of earthquake production and its application to earthquake clustering. J. Geophys. Res. 99 (18), 2601–2618.

Harris, R.A., 1998. Introduction to special section: stress triggers, stress shadows, and implications for seismic hazard. J. Geophys. Res. 103, 24347–24358.

Johnson, K.M., Segall, P., 2004. Imaging the ramp–décollement geometry of the Chelungpu fault using coseismic GPS displacements from the 1999 Chi-Chi, Taiwan earthquake. Tectonophysics 378, 123–139.

Ma, K.-F., Chan, C.-H., Stein, R.S., 2005. Response of seismicity to Coulomb stress triggers and shadows of the 1999 $M_w = 7.6$ Chi-Chi, Taiwan, earthquake. J. Geophys. Res. 110. http://dx.doi.org/10.1029/2004JB003389.

McGuire, R., 2001. Deterministic vs. probabilistic earthquake hazard and risks. Soil Dyn. Earthquake Eng. 21, 377–384.

Molchan, G.M., 1990. Strategies in strong earthquake prediction. Phys. Earth Planet. Inter. 61, 84–98.

Toda, S., Enescu, B., 2011. Rate/state Coulomb stress transfer model for the CSEP Japan seismicity forecast. Earth Planets Space. http://dx.doi.org/10.5047/eps.2011.01.004, 63, 171-185.

Toda, S., Stein, R.S., 2002. Response of the San Andreas fault to the 1983 Coalinga-Nuñez earthquakes: an application of interaction-based probabilities for parkfield. J. Geophys. Res. 107. http://dx.doi.org/10.1029/2001JB000172.

Utsu, T., 1961. A statistical study of the occurrence of aftershocks. Geophys. Mag. 30, 521–605.

Wiemer, S., Wyss, M., 2000. minimum magnitude of completeness in earthquake catalogs: examples from Alaska, the Western United States, and Japan. Bull. Seismol. Soc. Am. 90 (4), 859–869.

Wu, Y.M., Chiao, L.Y., 2006. Seismic quiescence before the 1999 Chi-Chi, Taiwan Mw7.6 earthquake. Bull. Seismol. Soc. Am. 96, 321–327.

Wu, Y.M., Chang, C.H., Zhao, L., Teng, T.L., Nakamura, M., 2008. A comprehensive relocation of earthquakes in Taiwan from 1991 to 2005. Bull. Seismol. Soc. Am. 98, 1471–1481. http://dx.doi.org/10.1785/0120070166.

Yen, Y.T., 2002. Slip distribution of $M_w > 6.0$ aftershocks of the 1999 Chi-Chi Taiwan earthquake. M.Sc. Dissertation, Natl. Cent. Univ., Taiwan, p. 122.

Yen, Y.T., Ma, K.F., 2011. Source-scaling relationship for M 4.6–8.9 earthquakes, specifically for earthquakes in the collision zone of Taiwan. Bull. Seismol. Soc. Am. 101 (2). http://dx.doi.org/10.1785/0120100046.

Yu, S.-B., Hsu, Y.-J., Kuo, L.-C., Chen, H.-Y., 2003. GPS measurement of postseismic deformation following the 1999 Chi-Chi, Taiwan, earthquake. J. Geophys. Res. 108, 2412. http://dx.doi.org/10.1029/2003JB002396.

Yue, L.-F., Suppe, J., Hung, J.-H., 2005. Structural geology of a classic thrust belt earthquake: the 1999 Chi-Chi earthquake Taiwan ($M_w = 7.6$). J. Struct. Geol. 27, 2058–2083. http://dx.doi.org/10.1016/j.jsg.2005.05.020.